JTTEE5 16:140–152
DOI: 10.1007/s11666-006-9006-3
1059-9630/$19.00 © ASM International

Peer Reviewed

Effect of System Parameters on Metal Breakup and Particle Formation in the Wire Arc Spray Process

N.A. Hussary and J.V.R. Heberlein

(Submitted January 14, 2006; in revised form May 11, 2006)

The significance of metal atomization in the wire arc spray process is directly related to the final coating quality produced. Since the early observations of the melting behavior of the wire tips by Steffens, relatively little has been done to further the understanding of the mechanisms involved. The primary atomization of the molten wire tips show existence of sheets and extrusions on both electrodes, which are strongly dependent on the system operating parameters. High-speed imaging has been used in this study, for classification of sheet, membrane and extrusion formations as a function of atomizing gas pressure, voltage and current settings. The breakup of metal structures formed on the electrodes is further classified in a manner consistent with established classifications for the break-up of other liquids, e.g., water or fuel. Quantitative descriptions of metal sheet lengths and breakup times are presented. The improved understanding of the metal breakup mechanisms in the wire arc spray process may provide a basis for (a) modification of existing computational codes for prediction of particle sizes and trajectories, and (b) for modifications to torch designs for providing more uniform particle fluxes.

Keywords coating quality, melting, metal atomization, metal breakup mechanisms, wire arc spraying

1. Introduction

The wire arc spray process has gained significant market share in the thermal spray industry; however, basic knowledge of the workings of the system hinders sophisticated developments of process controls for higher end applications. Steffens early work in the 1960s highlighted the differences of the liquid metal structures that exist at the electrode tip during the early stages of droplet formation (Ref 1). Such features were also observed by both Wang and Sheard in the mid-1990s using laser strobe photography (Ref 2, 3). Kelkar et al. latest developments in the wire arc process, based on the above mentioned studies, concentrated on studying the physics of the arc in cross flow, the fluid dynamics of the jet and predictions of droplet sizes and velocities (Ref 4, 5). Due to the lack of detailed understanding of the primary atomization process, Kelkar attempted to model the system basing his work on the well studied fields of welding and the traditional liquid atomization studies. Others such as Bolot et al. concentrated on three dimensional modeling of the fluid dynamics of the process (Ref 6). Varacalle et al. modeled the particle transport in the plume of the wire arc spray torch using computer codes to simulate the arc and the jet (Ref 7). More recently attempts at uncovering the extent of the interaction of the arc and the wire electrode tips have demonstrated the dramatic differences in the arc attachments at the two electrodes and their subsequent effect on the metal melting and primary atomization (Ref 8). The influence of the complex geometry of this system on droplet formation has also been pointed out. It was also suggested that control of this process has to be achieved at the first stages of particle formation so as to control the particle sizes and trajectories as they are issued from the wire tips. Recent studies demonstrated the differences of the size distributions of particles originating from the cathode and from the anode by using wires of different materials, and using in-flight diagnostics as well as analysis of the coating (Ref 9, 10). Size distributions as well as trajectories were found to be different for the particles emanating from the anode wire and from the cathode wire, but no relation to the atomization process was presented. Therefore, this study will present the mechanisms involved in the primary atomization of liquid metal from the wire tips and the effects of the process parameters on these mechanisms. Quantitative results of sheet, extrusion and membrane lengths, and breakup times will also be presented.

N.A. Hussary, Thermadyne Holdings, Inc., West Lebanon, NH; and **J.V.R. Heberlein,** University of Minnesota, Minneapolis, MN. Contact e-mail: nah@me.umn.edu

2. Experimental Setup and Analysis Technique

Praxair TAFA, Concord, NH, spray equipment has been used. A PB400 wire arc gun with a Mogularc 400R constant voltage power supply and a PF400R wire feed

unit were employed in all the experiments. A 1.6 mm (14 gage) diameter steel wire has been used (TAFA 30T Medium Carbon Steel) with the following composition: 0.12%C, 1.75%Mn, and 0.1%Cu with Fe as the balance. The melting point of this material is 1,809 K. Nitrogen has been used as the atomizing gas. A standard butterfly shaped commercial nozzle, supplied with the system, has been used. The operating parameters used in the experiments are shown in Table 1. The volume and mass flow rates of the gas, for a given system pressure setting, are shown in Fig. 1. The pressure gage and flow meter locations with respect to the torch head are shown in Fig. 2. High-speed photography was used to capture the events that occur at the wire electrodes. A high-speed camera (KODAK EKTAPRO HS Motion Analyzer, Model 4540, North Star Imaging, St. Paul, MN), capable of up to 40,500 frames/s, has been used. Various magnification lenses were fitted onto the camera to adjust the field of view. High intensity halogen lamps along with neutral density filters were used in a backlighting configuration as shown in Fig. 3. This setup reduced the high intensity light from the arc. The wires, liquid metal sheets, and the droplets became visible as their shadow imprinted on the CCD of the high-speed camera. The images were initially stored in the high-speed camera's processing unit and then transferred to a computer for analysis.

Table 1 A list of operating parameters and range of settings used in the current experiments

	Min	Max
Voltage	30 V	36 V
Current	100 A	300 A
Pressure	69 kPa	207 kPa

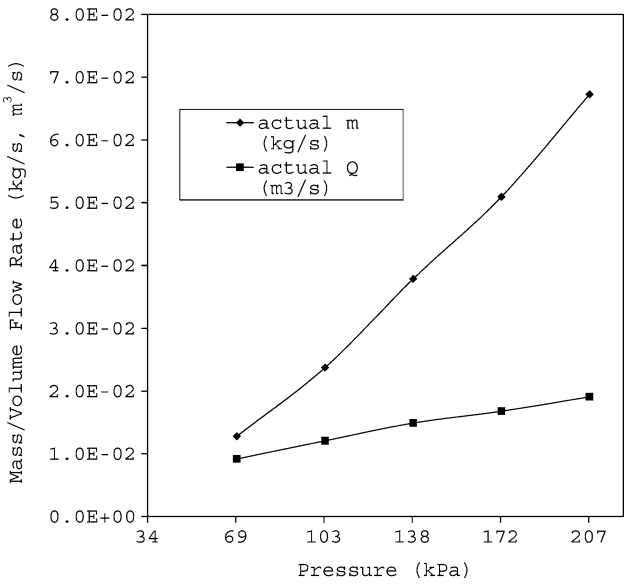

Fig. 1 Volume flow rate and mass flow rate of the nitrogen gas in the wire arc spray process as a function of system pressure setting

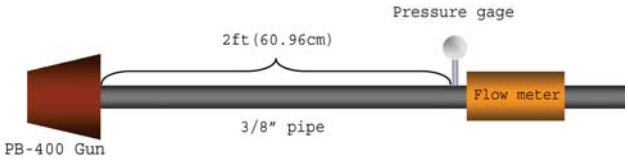

Fig. 2 Schematic of the torch, the pressure gages and flow meter. The pressure gage closest to the torch head is set as the system operating pressure

All the images in this study have been captured at a framing rate of 18,000 frames/s. The image exposure time is simply the inverse of the framing rate, i.e., 55 μs. The image resolution is 25,564 pixels. The voltage trace of the arc was also collected and was synchronized with the high-speed images using an HP54540A oscilloscope. Image analysis software has been used to extract quantitative information. All the results presented in this study are based on detailed analysis of 2000 consecutive images as well as visual observations of more than 10,000 images at each operating condition.

Final particle size distributions resulting from this process have been characterized. The particles were first collected by spraying into a container of compacted crushed ice while the torch was translated in front of the container at 2.5 cm/s. The particles were then dried and washed with alcohol to minimize rusting. The particles were then separated into 13 mesh sizes using Gilson (Lewis Center, OH) sieves and SS-3 Shaker. The mass at each mesh was measured and a mass fraction distribution was calculated. The mass mean diameter was calculated as an average representative number: $d_{\mathrm{mm}} = \sum m_i d_i / M$, where m_i is the mass of all particles in group i, d_i is a characteristic diameter of group i, and M is the total mass of the collected particles.

Coupons (3×5 cm) of aluminum and mild steel were sprayed with the wire described above for coating quality evaluation. The current was varied from 100 to 300 A, the voltage from 30 to 36 V and the pressure from 90 to 365 kPa. The samples were mounted on a rotating wheel in front of the torch at a distance of 10 cm. The tangential velocity of the samples was 3.5 cm/s. The samples were sectioned, mounted in epoxy and polished. Micrographs of the sectioned samples were taken with an optical microscope. The images were then analyzed by looking at the grayscale level after a background flat field correction to determine the percent porosity and oxide on each micrograph. Each data point presented is an average of 40 micrographs of four samples taken at each particular running condition.

3. Results and Discussion

3.1 Classifications of Breakup Mechanisms

Extensive studies have been performed on the liquid atomization phenomenon (Ref 11, 12). Although the fun-

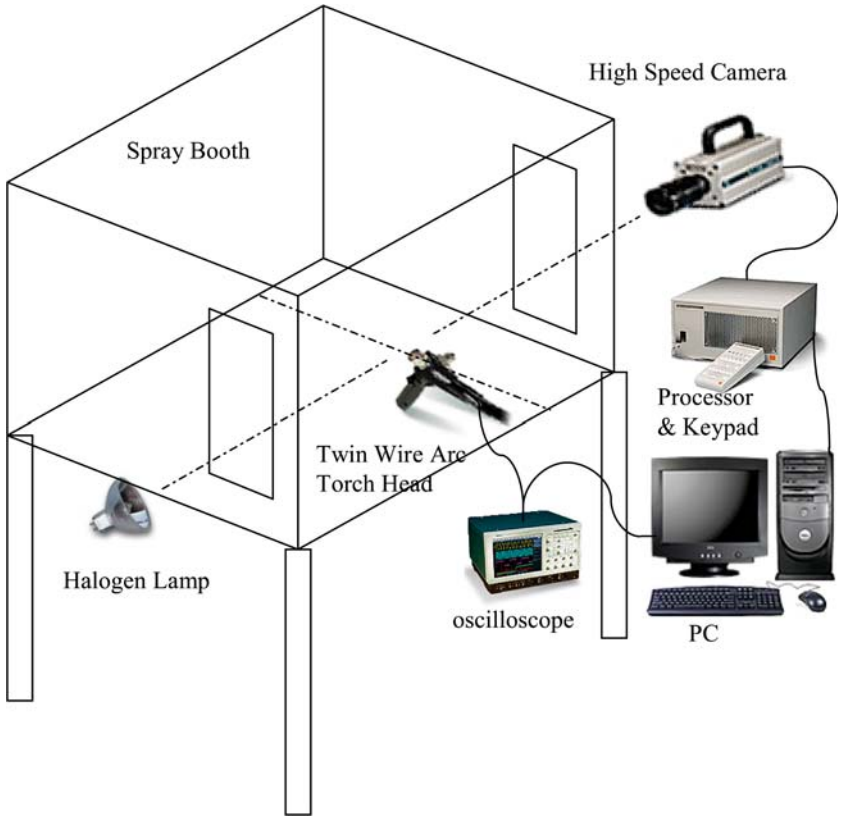

Fig. 3 Experimental setup of the high-speed camera with a halogen lamp as a backlighting source. The camera is directly connected to a computer for data storage and analysis

damental physical mechanisms of liquid breakup (jets and/or sheets) into drops have not been fully established, there seems to be an agreement that the important factors are liquid properties (viscosity, surface tension and density), gas properties and the relative velocity between the liquid and the atomizing gas (Ref 13). Although somewhat simplified, the classical picture of liquid breakup presented by Dombrowski and Johns occurs as a disturbance on the liquid surface which is enhanced by aerodynamic forces leading to the formation of ligaments (larger liquid drops), which may break up into smaller drops (Ref 14). The drops may also breakup further into even smaller ones (secondary atomization). Their analysis was based on the wave growth of the Kelvin-Helmholtz instability (Ref 15). Classifications of the various disintegration mechanisms in jets and sheets have also been reported (Ref 16-18). The aerodynamic atomization of the liquid jets (a liquid jet coflowing with a high velocity gas stream) was shown to have two important non-dimensional numbers, the liquid Reynolds number $Re_l = U_l d_l / \nu_l$ and the aerodynamic Weber number $We = U_{rel}^2 l_l \rho_g / \sigma_l$, where U_l, d_l, ν_l, σ_l are the liquid jet velocity, jet diameter, kinematic viscosity and surface tension, U_{rel} is the relative velocity between the liquid jet and the gas stream and ρ_g is the density of the coflowing gas. The classifications of the liquid jet breakup shows that there are four main categories: axisymmetric Rayleigh breakup ($We < 15$), Non-axisymmetric Rayleigh breakup ($15 < We < 25$), membrane breakup ($25 < We < 70$) and fiber type breakup ($100 < We < 500$). A compilation of the breakup mechanisms of liquid sheets as a function of the same parameters were also presented by Lasheras and Hophinger (Ref 19). They showed that the Rayleigh axisymmetric breakup mechanisms can occur up to $We \sim 10$ and Rayleigh non-axisymmetric breakup can occur up to $We \sim 100$ and the membrane breakup can occur up to a value of $We \sim 300$. These breakup processes will be described below in conjunction with the observation on the current process under investigation.

Previous studies on the wire arc spray process have shown that the constricted cathode attachment and diffuse anode attachment lead to different melting behaviors of the electrode wires and different molten metal structures at the edge of the wires (Ref 8). The structures of metal formed at the electrode edge are a combination of sheets, membranes and small extrusions, as seen in Fig. 4. Breakup of metal sheets, membranes and extrusions from the wire electrodes has been categorized into three types: (1) Rayleigh axisymmetric breakup; (2) Rayleigh non-axisymmetric breakup; and (3) membrane type breakup. These breakup mechanisms are graphically shown in Fig. 5. When the molten metal on the wire electrode is stretched in the direction parallel to the jet axis the forces acting on the liquid sheet in opposing directions lead to its breakup. Disturbances on the liquid metal/gas interface

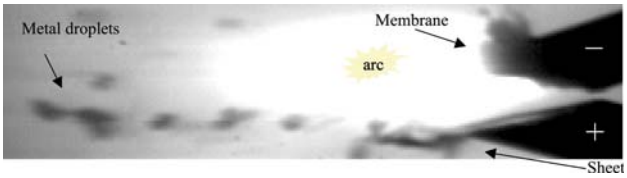

Fig. 4 A high-speed image demonstrating the formation of metal membrane on the cathode edge. The anode sheet is seen disintegrating into droplets (V = 36 V, I = 300 A, P = 69 kPa)

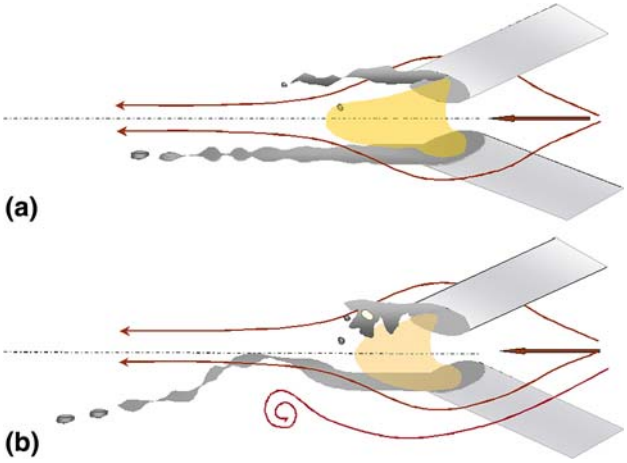

Fig. 5 Graphics demonstrate three types of liquid sheet/membrane breakup mechanisms. (a) Axisymmetric breakup mechanism shown on both electrodes. (b) Non-axisymmetric breakup mechanism shown on lower electrode and membrane type breakup mechanism shown on upper electrode

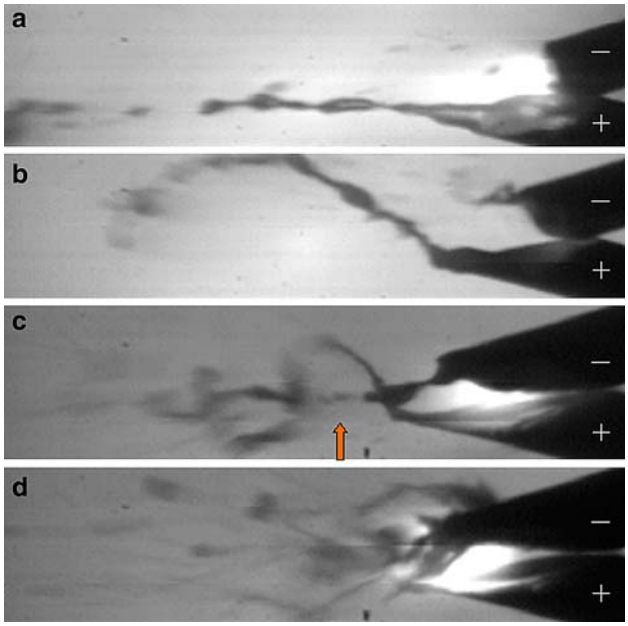

Fig. 6 High-speed images showing sheets, extrusions, and membranes at the edge of the wire electrodes as they disintegrate. (a) The anode sheet is disintegrating with Rayleigh axisymmetric type breakup. Resulting droplets travel parallel to the jet axis. (b) A highly curved anode sheet is disintegrating with a Rayleigh non-axisymmetric breakup type. The resulting droplets travel in the down stream directions with varying trajectories. (c) An upward traveling eddy in the flow causes the anode sheet to bend upwards resulting in a non-axisymmetric type breakup of the sheet. (d) The cathode sheet is seen to disintegrate by the membrane type breakup with holes forming in the membrane. The resulting strings of metal eventually breakup with axisymmetric and non-axisymmetric type break up.

are amplified leading to the formation of the Kelvin-Helmholtz type instability. Under the aerodynamic drag force, acting in the down stream direction, and the surface tension forces, acting in the upstream direction, the semi-hemispherical liquid metal, forming as a result of the amplified Kelvin-Helmholtz instability, breaks into droplets with trajectories parallel to the jet axis, as seen in Fig. 5(a). Such breakup mechanism is referred to as the Rayleigh axisymmetric breakup type. Due to the complex flow structure generated in the jet shear layer, the wake of the wires and the arc, an added force, acting in the transverse direction to the sheet resulting from the convecting eddies, leads to bends in the molten metal sheet and a flapping movement is seen as the sheet breaks up (Fig. 5b). Such mechanism is termed the Rayleigh non-axisymmetric breakup type. The membrane type breakup is observed when the sheet is thinly stretched at the edge of the wire electrode to a point were a hole starts forming at its center (Fig. 5b). The high viscosity, high surface tension liquid metal [carbon steel at its melting point has a viscosity 5 times larger than the viscosity of water, and a surface tension 26 times larger (Ref 20)] starts collecting at the rims of the membrane, around the newly formed hole, ultimately forming a molten metal ring that breaks up in the flow direction with either the Rayleigh axisymmetric or Rayleigh non-axisymmetric breakup mechanisms. High-speed images of the breakup types are shown in Fig. 6(a) to (d).

3.2 Effect of Operating Parameters

As one might expect, operating parameters have a significant effect on the type of breakup mechanism responsible for particle generation in the primary atomization stage. The importance of the various breakup types have been measured as a percentage of the time such mechanisms occur for an examination interval of 2000 consecutive frames. These effects have been examined for both the cathode and the anode. The significance of the breakup type on the disintegration of the anode sheet is shown in Fig. 7(a) and (b). Note that the most dominant breakup mechanism is the non-axisymmetric breakup type. It is especially important at low voltages. At 30 V the non-axisymmetric breakup spans the range of 50-90% with least dominance at the coordinate: 207 kPa and 100 A. While the non-axisymmetric breakup mechanism loses some dominance at high voltage, this diminishing importance is most noticeable at low pressures. It is believed that the influence of large-scale turbulence that contributes to the flapping movement of the sheets is less effective at low pressures. The decrease in the flapping

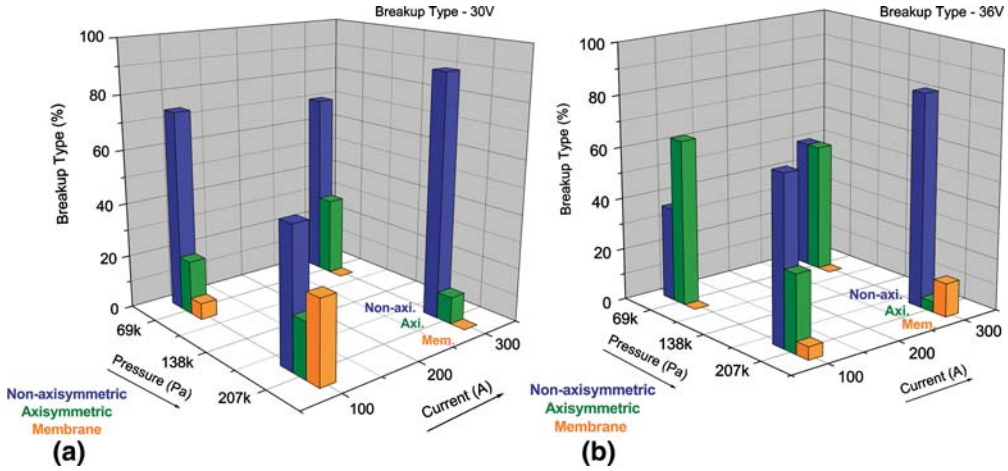

Fig. 7 Representation of the effects of the process parameters on the breakup type of the anode sheet. The *z*-axis represents the percentage of the time a breakup mechanism is observed: (a) 30 V; (b) 36 V

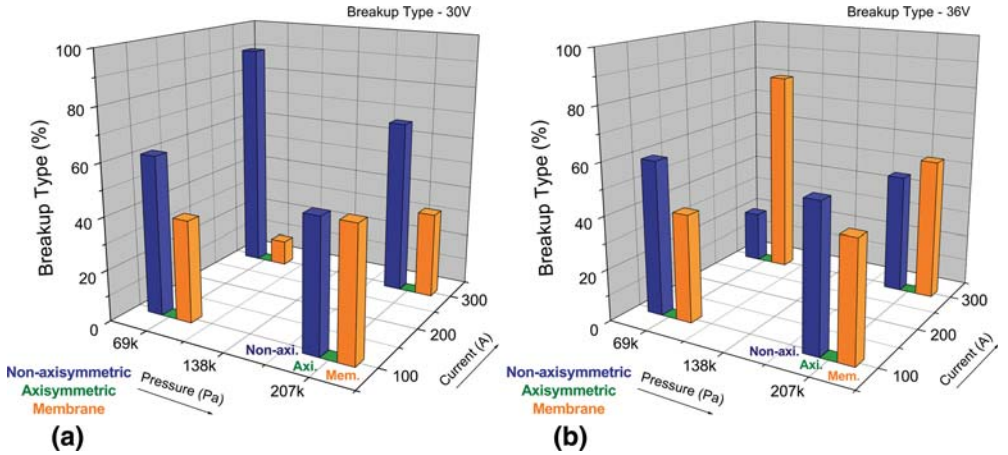

Fig. 8 Representation of the effects of the process parameters on the breakup type of the cathode sheets. The *z*-axis represents the percentage of the time a breakup mechanism is observed: (a) 30 V; (b) 36 V

movement of the sheets were evident in the high-speed images. An opposite effect is observed when examining the axisymmetric breakup mechanism. Note that axisymmetric breakup gains significance at higher voltages and is especially important at low pressures. The membrane type breakup has the least significance of all the breakup processes and no particular trend is readily seen. It is believed that the increase in size of the arc (which was clearly seen in the high-speed images) between the electrodes, at higher voltages, is a significant factor in determining the breakup mechanism. As the arc fills the wake behind the wires and between the electrode sheets, the large eddy structure of the jet pushing on the sheet in the transverse direction has less of an effect of deflecting and bending the liquid metal sheet. This reduces the dominance of the non-axisymmetric breakup and increases that of the axisymmetric breakup mechanism. While no modeling work has been performed to show the effect of the large wake effect behind the wires and the arc, initial flow visualization of the cold flow (no arc present) show a significant wake behind the wires.

The effect of the operating parameters on the breakup of the metal from the wire cathode is shown in Fig. 8(a) and (b). The non-axisymmetric breakup mechanism is the most dominant at the cathode, especially at low voltage and low pressure, with frequency ranging from 50 to 90% of the time. This behavior is similar to the anode case. With increased voltage the non-axisymmetric breakup mechanism decreases in importance especially at higher currents—little change in values is seen at lower currents. Since the axisymmetric breakup mechanism is hardly observed at the cathode, the non-axisymmetric breakup type competes with the membrane type breakup. The frequency of occurrence of the membrane type breakup increases with increasing voltage and it becomes especially important at higher currents. Since an increased current translates into an increased amount of molten material, the cathode sheet increases in length at higher currents, as will be discussed in subsequent sections. The sheathing and thinning of the larger sheets causes holes to form at their center and the formation of small molten metal strings. With a smaller sheet, however, breakup occurs

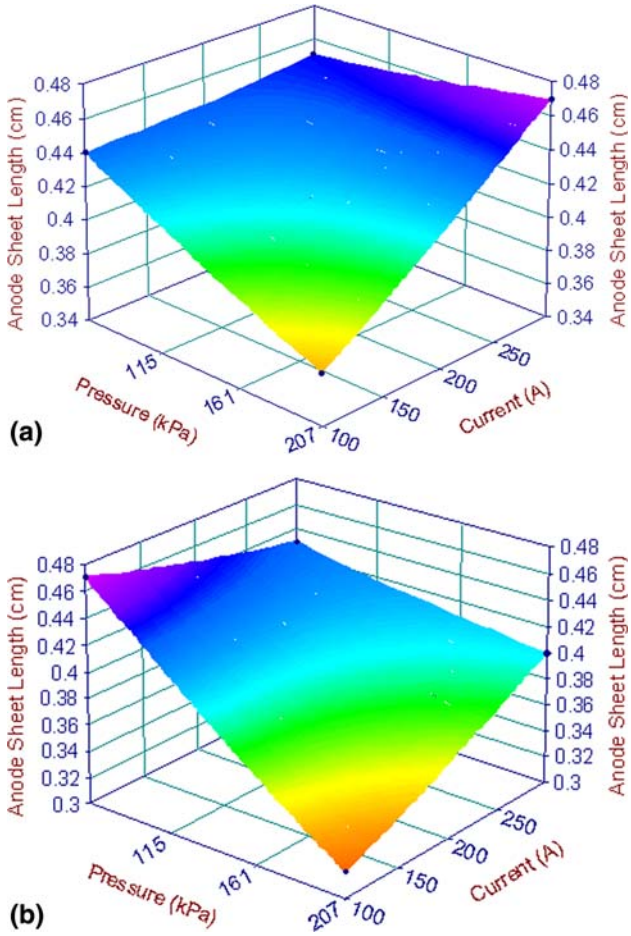

Fig. 9 Anode sheet length as a function of pressure and current: (a) 30 V (top); (b) 36 V (bottom)

much before the hole can develop in the middle of the sheet leading to non-axisymmetric breakup.

3.3 Sheet Length and Breakup Time

Electrode sheet lengths and breakup times have been quantified using high-speed images. The lengths and breakup times are presented in 3-D graphs as a function of the operating gas pressure and current setting. Each graph is given at different voltage settings of either 30 or 36 V. The importance of these parameters lies in their influence on the size of the produced drops after the primary atomization and subsequently the final particle sizes after the secondary atomization phase. The electrode sheet length has been defined as the length of the sheet from the edge of the electrode to its farthest end just before it breaks up. The electrode breakup time is defined as the time from the breakup of one sheet to the next.

The anode sheet lengths are presented in Fig. 9(a) and (b). The anode sheet length values range between 3.2 and 4.7 mm. While the actual values of the sheet lengths have significant standard deviations, 20-40% of the average value, the general effects of the process parameters can be clearly seen. An increase in pressure causes a decrease in the sheet length, except at lower voltage and higher currents where a slight increase has been observed. This generally decreasing trend is expected since enhanced atomization accompanies increased gas velocity and mass flow rate. A current increase has an effect of increasing the sheet length except at higher voltage and lower pressures where a slight decrease in sheet length has been observed. The general trend of increasing sheet length with current is consistent with the fact that increased current is an indication of the amount of material being melted. In reality setting the current in this process sets the wire feed rate. A voltage increase causes an overall decrease in the anode sheet length. While an explanation of this behavior is not clear, one may speculate to the cause of this effect. Observations of the high-speed images show an increase in the size (length and diameter) of the arc with increased voltage and minimal increase in the distance between the electrodes. Consequently, the larger arc voltage allows an arc which is strongly bowed in the downstream direction, leading to a stronger heating of the atomizing gas rather than an increase in wire melt rate. The increase in the gas heating will result in higher gas velocities, which in turn may lead to shorter sheet lengths. It must be noted that the final particle size showed a slight increase with increasing voltage except at low currents. This is attributed to the breakup mechanisms at the anode, namely the axisym-

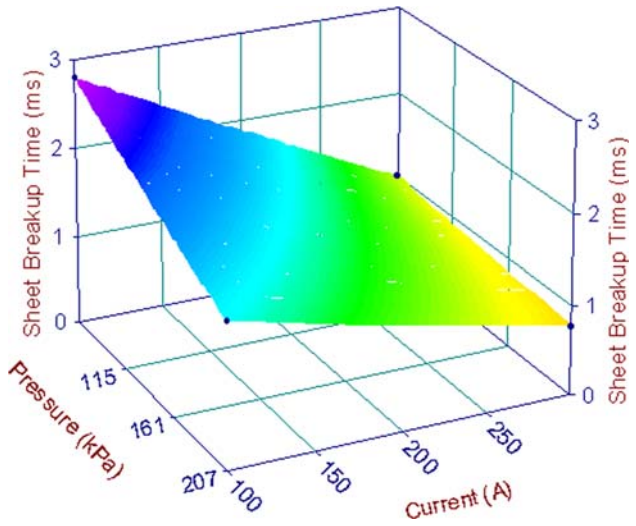

Fig. 10 Cathode sheet length as a function of pressure and current: (a) 30 V (top); (b) 36 V (bottom)

metric breakup mechanisms. Reports in the traditional liquid atomization literature indicate that resulting particles from axisymmetric breakup tend to be larger than those from the non-axisymmetric breakup. Final particle size will be discussed in subsequent sections.

Effects of the process parameters on cathode sheet length are shown in Fig. 10(a) and (b). Note that the values of the cathode sheet lengths are significantly smaller than the anode, except at higher currents and pressures where they are comparable. The cathode sheet length values span the range of 1.3-3.7 mm. While visually observing the length of the liquid metal structures at the end of the electrode, it was deemed appropriate to refer to structures less than 2.0 mm as extrusions rather than sheets. The standard deviation for the cathode sheet length also has a large range, 20-50% of the average length. A pressure increase has an effect of slightly decreasing the length of the cathode sheets/extrusions at lower currents while the opposite occurs at higher currents. This effect has been visually observed as a consolidation of all the little extrusions from the sides of the wire cathode to its front edge, therefore, forming a larger sheet rather than extrusions. A voltage increase has an overall effect of decreasing the sheet/extrusion length, an observation that is consistent with that of the anode sheet.

The sheet breakup times for the anode range between 0.63 and 2.8 ms as seen in Fig. 11. The standard deviations of the anode sheet breakup time range between 30 and 80% of the average values. The process parameters have predictable effects on the anode sheet breakup time. An increase in atomizing gas pressure causes a decrease in the anode sheet breakup time, i.e., prompt breakup with increasing gas velocity and mass flow rate (increasing momentum). An increased current has an effect of decreasing breakup time, which is caused by an increase in the melting rate of the metal. An increased voltage, however, causes an increase in breakup time. While this effect is not fully understood, the increased voltage, i.e., power

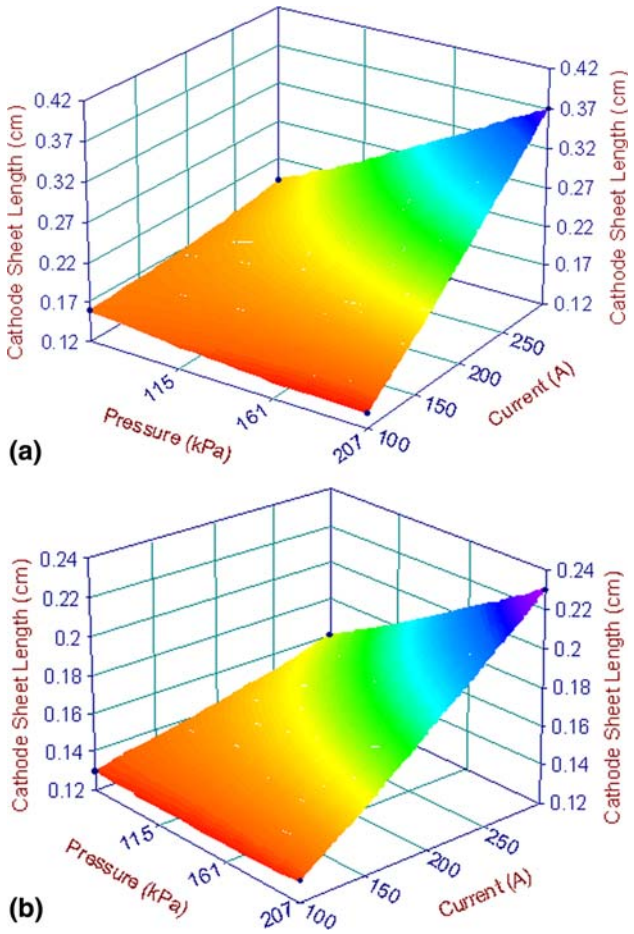

Fig. 11 Anode sheet breakup time as a function of pressure and current at 30 V

input, does not seem to increase the melting rate but rather dissipates in the arc. The cathode breakup times also exhibit behavior similar to that of the anode. The breakup time ranges from 0.48 to 0.90 ms with 30-50% standard deviation (Fig. 12). Both an increase in pressure and voltage lead to a decrease in the breakup time of the cathode sheets/extrusions. However, the current seems to have little influence on the breakup time, an effect that might be compensated by the increase of the sheet length. Estimation of the mass contained in the sheet was not possible since the sheet width and thickness were not measured due to the movement and rotation of the electrodes and therefore the obstruction of one or two of these dimension due to the viewing angle. In general not only are the trends important but also the actual values of both the sheet length and the breakup time. These values should be considered together since a slight increase or decrease of one (i.e., sheet length) could be masked by the other (i.e., breakup time: a significant decrease in time indicating a significant increase of frequency of breakup). This is particularly important since both the sheet length and the breakup time have significant standard deviations as pointed out above. A general formulation of the main trends showing the effects of the process parameters on the anode sheet length can be summarized in the following

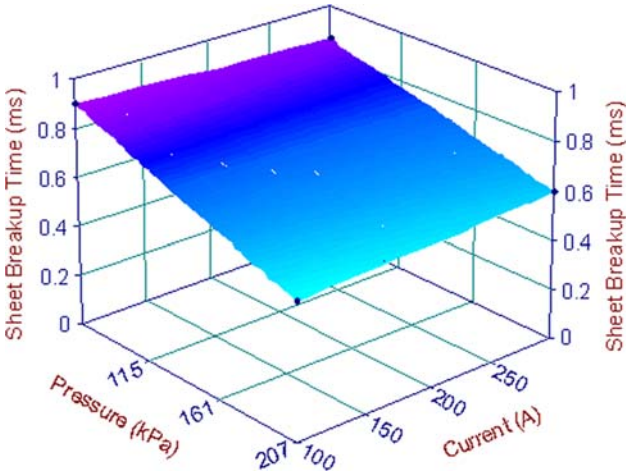

Fig. 12 Cathode sheet breakup time as a function of pressure and current at 30 V

form: $L \sim P^{-a} I^{b} V^{-c}$, where a, b, and $c > 0$. Note that these formulations are not a fit of the data shown but rather an aid to help elucidate those trends. Similarly such formulations can be devised for both electrode sheets and breakup times. Table 2 shows a summary of such relations.

3.4 Effect of Jet Flow Structures

The flow structures in the jet have a pronounced effect on the liquid metal atomization both in the primary and secondary stages. As discussed previously, large structures in the jet are seen to affect the liquid metal sheet at the edge of the electrodes. Large eddy structures in the flow field have also been observed by noting the movement of the anode and cathode sheets, as seen earlier in Fig. 6. Although these images are not consecutive frames they demonstrate the formation process of the molten sheet structure. As the sheet starts to extend to a certain critical length the aerodynamic effect on the sheet increases by producing bends in the sheet. These bends increase in size, as they are carried downstream and further turn with the large eddy structure of the flow. As the flapping movement and bending of the liquid metal sheet continues a critical point is reached at which the surface tension forces cannot hold the bending shapes of the metal resulting in the formation of showers of droplets. Such breakup mechanisms have been identified in the previous section as a non-axisymmetric breakup type. The eddy structures behind the wires, especially in the momentary absence of

Table 2 Formulation of operating parameter effects on electrode sheet length and breakup time

Electrode	Sheet length	Breakup time
Anode	$L \sim P^{-a} I^{b} V^{-c}$	$\tau \sim P^{-d} I^{-e} V^{f}$
Cathode	$L \sim P^{g} I^{h} V^{-i}$	$\tau \sim P^{-j} V^{-k}$

Note: The constants a through k are real positive numbers.

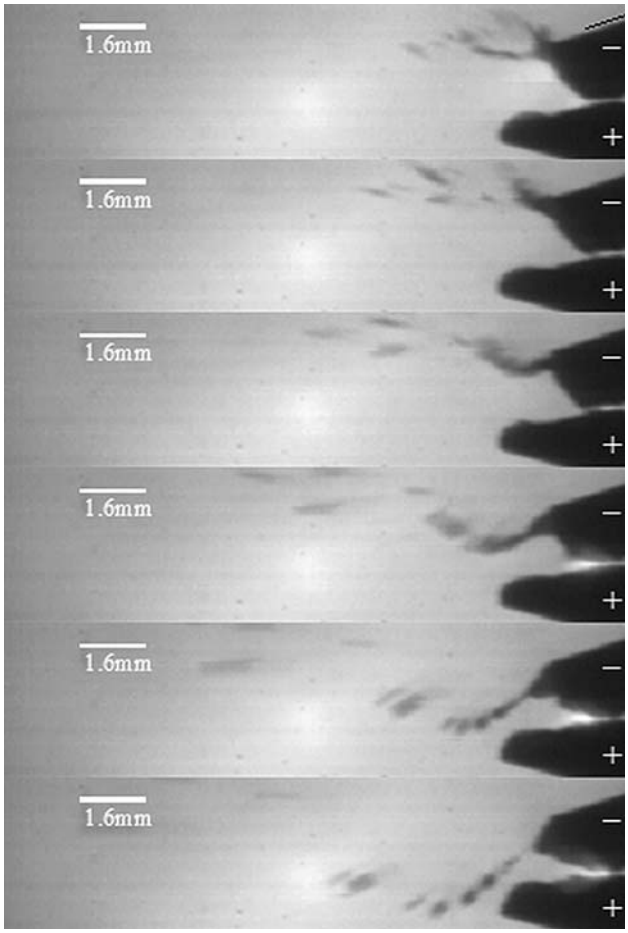

Fig. 13 A series of images showing the effect of the large flow structure on the breakup up of the cathode sheet and the dramatic direction change of the produced particles. Parameters: V = 30 V, I = 100 A, and P = 69 kPa. Note that every other image of the sequence have been shown. A framing rate of 18,000 frames/s has been used.

the arc, have a significant effect on the primary atomization of the sheets/extrusions. As can be seen in Fig. 13, the cathode (top electrode) sheet starts breaking with a membrane type mechanism, forming a ring, with the particles detaching and moving in the upward direction. As more metal is moved forward to the cathode edge, the large flow structures, in the wake of the wires, act in a downward direction causing a bend in the sheet and a downward motion of the metal. The sheet breaks up and the particles gain velocity with a downward direction. Such drastic changes in the motion of the sheet and the resulting droplets are a strong indication of the significance of the flow structure in the jet, its shear layer and the wake behind the wires.

A similar effect is also seen on the anode sheet. Figure 14 shows the effect of the large eddy structures on the bending of the anode sheet thus determining its breakup mechanism. An important observation is the location of the bends/twists with respect to the arc location. Note that the bending of the sheet, shown in Fig. 14, is right down-

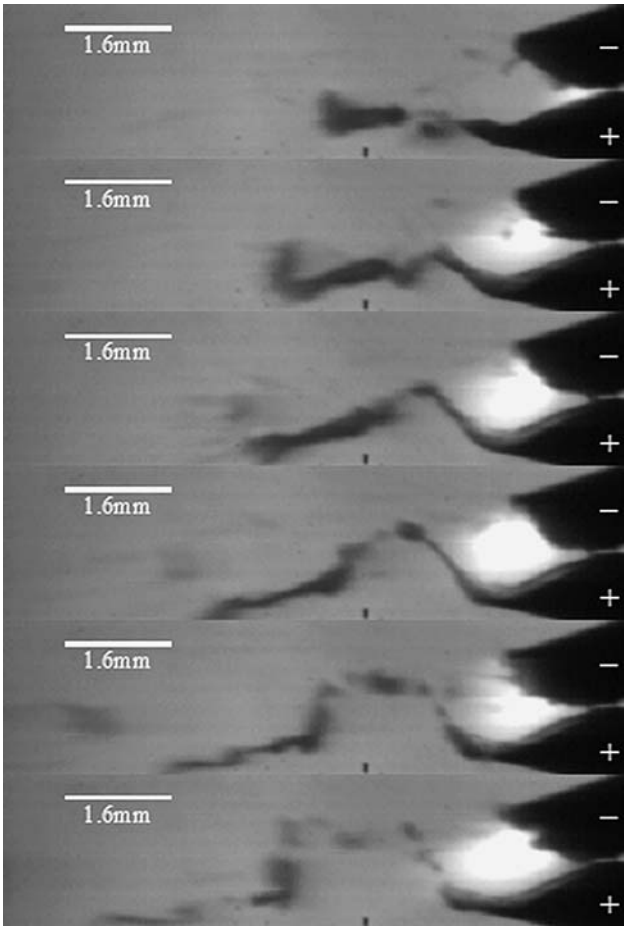

Fig. 14 A series of images showing the effect of the large flow structure on the breakup up of the anode sheet, the dramatic shape of the anode sheet and the subsequent direction change of the produced droplets. Parameters: V = 30 V, I = 100 A, and P = 207 kPa. Note that every other image of the sequence has been shown. A framing rate of 18,000 frames/s has been used.

stream of the arc indicating the obstruction of the fluid flow by the arc. The wake behind the wires and the arc, especially in the momentary absence of the arc due to its fluctuation, represents a low-pressure zone. When eddy structures in the flow move on the underside of the anode sheet the upward bending of the metal sheet is observed and the breakup of the anode sheet occurs by the non-axisymmetric breakup type. Therefore, the presence of the arc, especially an elongated one (higher voltage setting), minimizes the effect of the sheet bending and forces the sheet to disintegrate with axisymmetric breakup mechanism. The jet flow structures, therefore, work in coordination with the body of the arc in the wake of the wires to influence the sheet bending and flapping movement so as to determine the breakup mechanism. However, the effect of the flow structure is not limited to its influence on the primary breakup mechanism but also on the subsequent trajectories of the particles. Such influence has been shown in previous studies (Ref 8).

3.5 Metal Ejection and Arc Movement

The sheet formation on the anode and its subsequent disintegration is observed to be synchronized with the forward movement of the arc. This effect was first observed through the high-speed images. Correlation of the arc voltage and the high-speed images clearly show that as the arc moves forward and elongates the voltage increases. With the forward movement of the arc, the molten metal on the anode surface is swept to the leading edge of the wire thus forming the sheet. The long sheet is then disintegrated by one of the above mentioned mechanisms.

Figure 15 clearly shows the synchronization effect by comparing the voltage trace with the high-speed photography. Note that this observation has also been seen at the cathode. However, it is very important to note that while the arc forward movement causes ejection of metal from the cathode, the metal is also seen to detach when the arc is in the back position (not yet stretched forward).

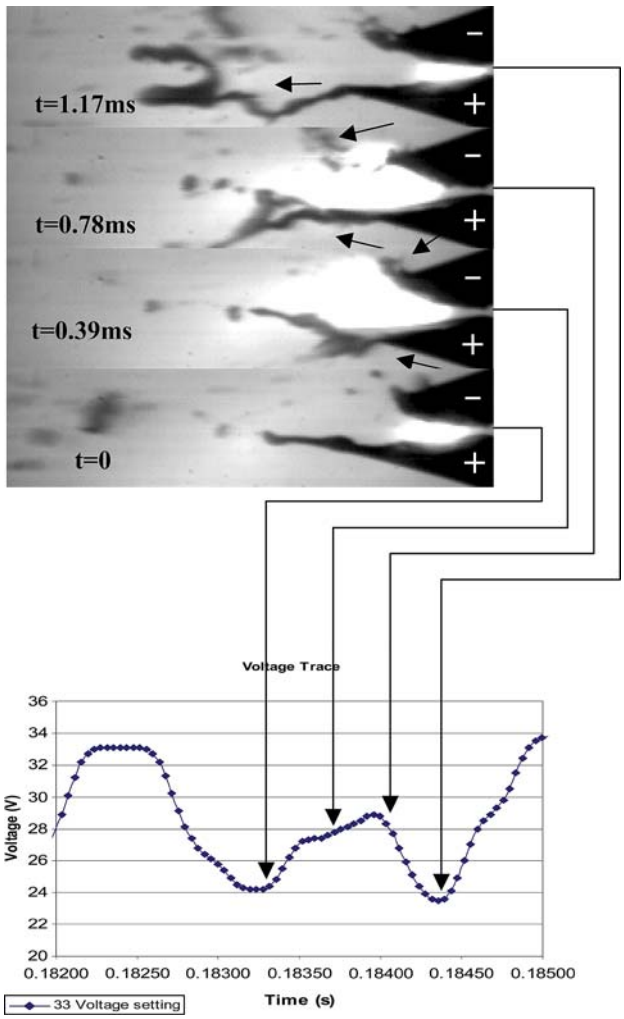

Fig. 15 Metal ejection from the anode is seen synchronized with the arc forward movement, which also corresponds to an increase in the arc voltage. Parameters: V = 33 V, I = 300 A, P = 69 kPa

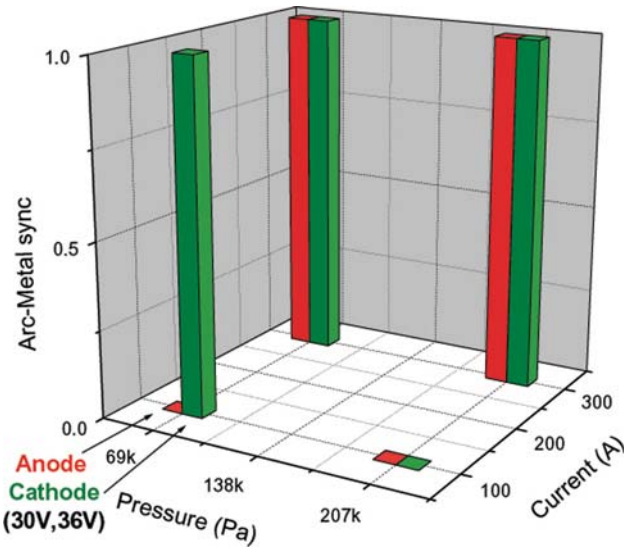

Fig. 16 Bar graph showing the synchronization of arc forward movement with metal ejection from both electrodes. The z-axis represents the fraction of the time such synchronization were observed

Quantification of this phenomena is shown in Fig. 16. This synchronization of the arc forward movement and the metal ejection is only observed at high currents (300 A) with any pressure and voltage setting. Therefore, prediction of metal ejection from the anode can be achieved, given a sufficiently high current setting, by monitoring the rising value of the arc voltage.

3.6 Final Particle Sizes

Ultimately, the quality of the deposit produced by this system is dependent on the properties of the particles, i.e. their sizes, speeds and temperatures. Manipulation of such properties has been successfully demonstrated in other studies (Ref 21). It is important, however, to establish a correlation between the primary atomization stage and the final particle sizes produced in this process. Figure 17 shows a sample particle size distribution. The shape of the particle size distribution varied from bimodal/multi-modal distribution towards single modal distribution when decreasing the upstream pressure. This change reflects the difference in droplet sizes leaving the electrodes. High-speed images show smaller extrusions and smaller droplets detaching from the cathode at high pressures. This has been reported in previous work and visually confirmed in this current study (Ref 5). However, the extent of the contribution of the detachment mechanisms from the electrodes or the secondary atomization on the various peaks is not clear. The effect of the process parameters on the particle sizes is shown in Fig. 18. An increase in pressure causes a decrease in the mass mean diameter (d_{mm}) due to the high relative velocity between the droplets and the gas. An increase in the current causes an increase in the particle d_{mm} because of the increase of the mass of the molten material per unit of available gas momentum. An increased voltage slightly increases d_{mm}. This effect is more pronounced at lower currents. When comparing the effects of the process parameters on both the d_{mm} and the electrode sheet lengths an agreement in general trends is clearly seen. Increasing the current and decreasing the pressure causes an increase in the electrode sheet lengths and an increase in the d_{mm}. Similarly, decreasing the current and increasing the pressure causes smaller anode and cathode sheets and a decrease in the d_{mm}.

The atomization process, as has been shown, can be quite complex due to the large number of variables present and the number of stages involved in the atomization process, including: (1) the metal melting at the cathode and the anode and the formation of sheets, extrusions and membranes; (2) the primary atomization stage with its various breakup mechanisms; and (3) the secondary

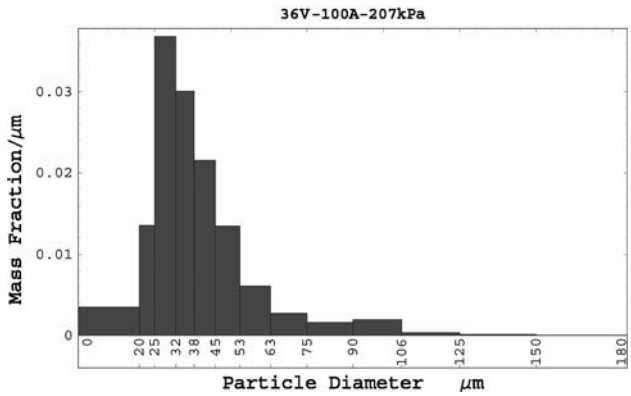

Fig. 17 Size distribution of particles collected from the wire arc spray process with the following operating parameters: 36 V, 100 A, and 207 kPa

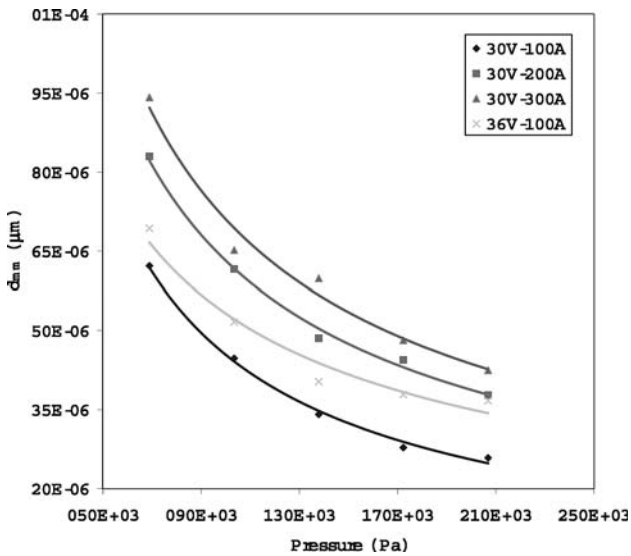

Fig. 18 Graphical representation of particle size in the wire arc process given a certain pressure and current setting

atomization stage (which has not been discussed here). One might expect, however, the primary atomization stage to have a strong effect on the final particle sizes produced. When viewing the value of the d_{mm} as a function of pressure, as shown in Fig. 18, one might reasonably assume that such curves might be collapsed onto a line with the proper considerations of the physical mechanisms discussed above. A reasonable approach would be to utilize the Weber number, $We = U_{rel}^2 L_s \rho_g / \sigma_l$, a non-dimensional number representing the aerodynamic forces to the surface tension forces that are involved in disintegrating sheets and drops, where U_{rel} is the relative velocity between the metal and the gas/plasma, L_s is a length scale representing the size of the disintegrating metal (note that the sheet thickness or a diameter would have been preferable for this value, however, the current experimental setup could not determine such value), ρ_g is the density of the gas/plasma and σ_l is the surface tension of the liquid metal. Determining these values might prove challenging due to the complexity of this process. A first order approximation of these values will be presented. A reasonable assumption for the value of the liquid metal surface tension is the value at the melting temperature of the metal. Since the velocity of the liquid metal sheets and ligaments are relatively small compared to the velocity of the gas and the plasma around it, one can assume then that the velocity term can be approximated with the velocity of the gas/plasma. However, the value of the gas/plasma velocity can be difficult to predict due to the added arc heating, arc fluctuations, jet-ambient mixing and location of sheet with respect to nozzle exit. In addition, two different flows surround the sheets, the hot high velocity low density plasma on the arc side and a relatively high density cold gas on the outside of the sheet. This is further skewed by the fact that most of the gas supplied in this process goes around the arc. Therefore, as a rough first estimate the value of the cold gas jet will be assumed. Similarly, the density of the gas is a function of the operating parameters and the location relative to the metal sheets and arc location. Therefore, for simplicity the cold gas density will be used. The length scale of the metal structures can be either the anode or cathode length or an average value. In this case, an average value will be taken. Figure 19 shows that the lines appearing in Fig. 18 collapsed onto a single line, with a correlation coefficient of 0.66, despite the gross simplifications used in evaluating the Weber number, thus illustrating the important effects of the primary atomization stage onto the final mass mean diameter and demonstrating a clear trend.

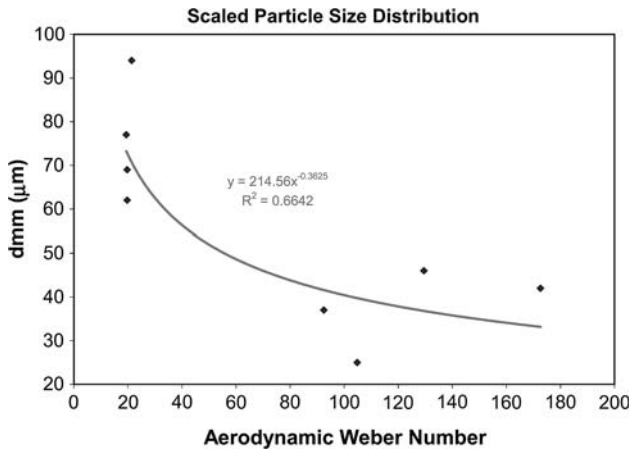

Fig. 19 Scaled particle size distribution showing the collapsed lines onto one line using the Weber number as a non-dimensional parameter

3.7 Coating Quality

The final determination of a successful coating is ultimately based on the attainment of a desired value of porosity and oxides for a particular application. Similarly, the microstructure of the achieved coating will assure the integrity of the deposit. Figure 20 shows the results of the image analysis of the sprayed samples at different operating conditions. The porosity at low pressures (90 kPa) of all the samples sprayed varied between 8 and 15% regardless of the current and voltage settings and are statistically indistinguishable. At higher pressure settings, the porosity increases with increasing current. This is consistent with the behavior of d_{mm} and the sheet lengths, each having larger values at increased current setting. While at a lower current setting an increase in pressure results in a decrease in porosity as expected, this is not the case at higher current levels were the porosity is statistically invariant with pressure. This may be consistent with the observation of large agglomerate of metal detaching from the electrodes at higher current level regardless of the pressure setting. The oxide content of the samples shows an increase with increasing pressure as expected. However, the spread in the data prohibits any solid conclusions regarding the effects of the current on the oxide content.

The sample micrographs shown in Fig. 21 clearly illustrate the difference in microstructure. At low current level and low pressure (Fig. 21a) one can see both large deformed droplets (an indication of large agglomerates detached from the anode) and small droplets (an indication of smaller drops detached from the cathode). As the current is increased while keeping the pressure low (Fig. 21b), the microstructure of the coating becomes more homogeneous formed mainly of large deformed droplets which directly relates to the large agglomerates of metal detached from both electrodes.

Increasing the pressure results in fine lamella microstructure the result of well atomized drops. The oxide content (seen as gray color matter) increases with pressure due to the increased metal-oxygen reaction given the larger surface area to volume of the finely atomized particles as well as the increased entrainment of the ambient air in the spray jet. It must be emphasized that these observations are valid for the particular nozzle geometry investigated, and that different nozzle designs generating different velocities at the wire tips may produce stronger pressure dependencies (Ref 2, 6). In particular, use of

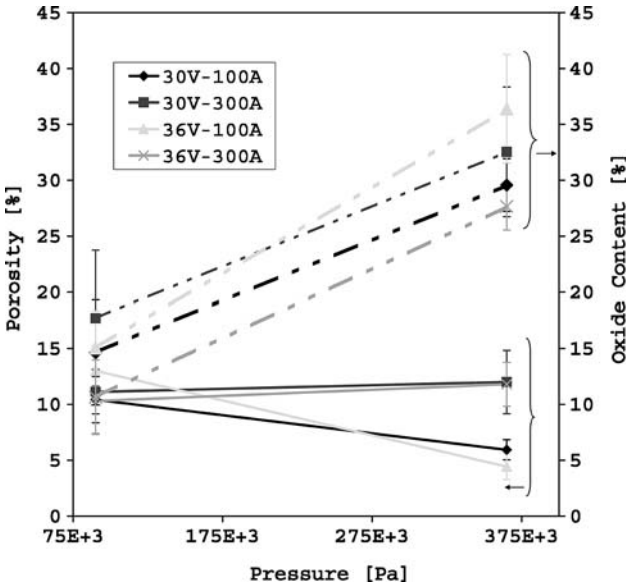

Fig. 20 Percent porosity and oxide content of samples sprayed at various operating conditions

shroud can minimize the oxidation as shown by Wang (Ref 2). While the breakup mechanisms and particle size distribution are important parameters affecting the coating quality, also the velocity of these particles is of prime importance and was not measured in this study.

4. Summary and Conclusions

While the wire arc spray process has been successful in the thermal spray industry, its penetration into the high precision and high quality coating applications has been slow due to the lack of fundamental knowledge to allow for better control of the system. Therefore, the goal of this study has been focused on the understanding of the primary atomization of the metal and the effect of the arc, fluid dynamics and process parameters on particle formation and coating quality.

The structures formed at the edge of the electrodes have been identified as either sheets, extrusions or membranes. Such structures disintegrate by three mechanisms: (a) Rayleigh axisymmetric breakup, (b) Rayleigh non-axisymmetric breakup, and (c) membrane type breakup. The system parameters determine the structures formed on the electrodes, their breakup mechanism and the final particle sizes and coating quality. For constant current and voltage, increasing the pressure results generally in shorter anode and somewhat shorter cathode sheet lengths, smaller particle sizes and denser coatings. For constant voltage and pressure, increasing the current results in larger anode and cathode sheets (particularly at higher pressures), larger particle sizes and denser coatings. For constant current and constant pressure, increasing the voltage results in decrease in sheet lengths of both electrodes and an increase in particle sizes (particularly at low currents). At low voltages, the non-axisymmetric breakup dominates, but at the higher voltage, more axisymmetric breakup is observed at lower pressures with the anode and more sheet breakup at the cathode. This variety in breakup mode may be the reason for the ambiguity in the effect of voltage changes on sheet length and particle diameter behavior.

Control of the particle size may be achieved by controlling the breakup mechanisms, which maybe accomplished by de-coupling the primary and the secondary atomization stages. Correlation exists between particle ejection and voltage trace behavior, which may be used for improved control.

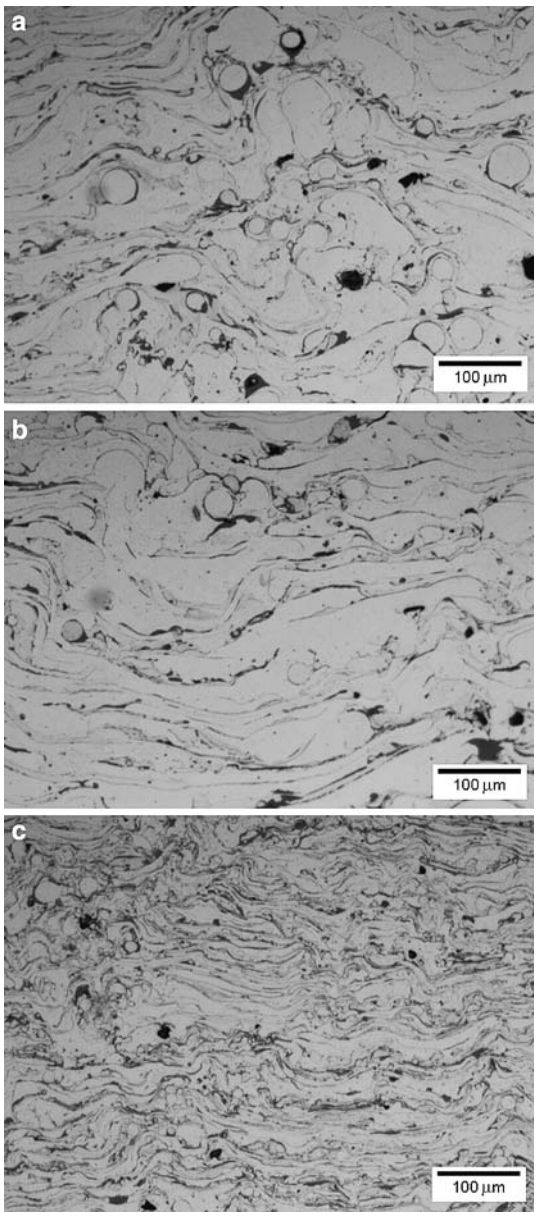

Fig. 21 Micrographs of the polished samples: (a) 90 kPa, 30 V, 100 A; (b) 90 kPa, 30 V, 300 A; (c) 365 kPa, 30 V, 300 A

Acknowledgment

Work supported by the University of Minnesota.

References

1. H.D. Steffens, Metallurgical Changes in the Arc Spraying of Steel, *Br. Weld. J.*, 1966, **13**(10), p 597-605
2. X. Wang, J. Heberlein, E. Pfender, and W. Gerberich, Effect of Nozzle Configuration, Gas Pressure, and Gas Type on Coating Properties in Wire Arc Spray, *JTST*, 1999, **8**(4), p 565-575
3. J.S.Sheard, J. Heberlein, K. Stelson, and E. Pfender, Diagnostic Development for Control of Wire-Arc Spraying, *Thermal Spray: A United Forum for Scientific and Technological Advances*, C.C. Berndt, Ed., Sept 15-18, 1997 (Indianapolis, IN), ASM International, 1998, p 613-618
4. M. Kelkar, N. Hussary, J. Schein, and J. Heberlein, Optical Diagnostics and Modeling of Gas and Droplet Flow in Wire Arc Spraying, *Thermal Spray: Meeting the Challenges of the 21st Century*, C. Coddet, Ed., May 25-29, 1998 (Nice, France), ASM International, 1998, p 329-334
5. M. Kelkar and J. Heberlein, Wire-Arc Spray Modeling, *Plasma Chem. Plasma Proc.*, 2002, **22**(1), p 1-25
6. R. Bolot and C. Coddet, Analysis of the Arc Spray Process via CFD, *Thermal Spray: Meeting the Challenges of the 21st Century*, C. Coddet, Ed., May 25-29, 1998 (Nice, France), ASM International, 1998, p 329-334
7. D.J. Varacalle, D.L. Hagarman, J.R. Fincke, W.D. Swank, V. Zanchuck, and E. Sampson, An SDE Study of Twin Wire Electric Arc Sprayed Nickel Aluminum Coatings, *Advances in Thermal Spray Science & Technology*, C.C. Berndt and S. Sampath, Ed., Sept 11-15, 1995 (Houston, TX), ASM International, 1995, p 373-380
8. N.A. Hussary and J.V.R. Heberlein, Atomization and Particle-Jet Interactions in the Wire-Arc Spraying Process, *JTST*, 2001, **10**(4), p 604-610
9. Y.L. Zhu, H.L. Liao, C. Coddet, and B.S. Xu, Characterization via Image Analysis of Cross-over Trajectories and Inhomogeneity in Twin Wire Arc Spraying, *Surf. Coat. Technol.*, 2003, **162**, p 301-303
10. M.P. Planche, H. Liao, and C. Coddet, In Flight Particles Analysis for the Characterization of the Arc Spray Process, ITSC 2005. ASM International, Materials Park, Basel, Switzerland, 2005
11. N. Chigier, *Energy Combustion and Environment* (New York), McGraw Hill, 1981
12. A.H. Lefebvre, Atomization and Sprays. Hemisphere Publ. Co, New York, 1989
13. Chigier, The Physics of Atomization, *Proc. of the Fifth Int. Conf. on Liquid Atomization and Spray Systems*, H.G. Semerjian, Ed. (Gaithersburg, MD), ILASS-Americas and NIST, 1991, p 49-64
14. N. Dombrowski and W.R. Johns, The Aerodynamic Instability and Disintegration of Viscous Liquid Sheets, *Chem. Eng. Sci.*, 1963, **18**, p 203-214
15. G.D. Crapper, N. Dombrowski, and G.A.D. Pyott, Kelvin-Helmholtz Wave Growth on Cylindrical Sheets, *J. Fluid Mech.*, 1975, **68**(3), p 497-502
16. Z. Farago and N. Chigier, Morphological Classification of Disintegration of Roud Liquid Jets in a Coaxial Air Stream, *Atomiz. Sprays*, 1992, **2**(2), p 137-153
17. S.P. Lin and R.D. Reitz, Drop and Spray Formationi from a Liquid Jet, *Annu. Rev. Fluid Mech.*, 1998, **30**, p 85-105
18. A. Mansour and N. Chigier, Disintegration of Liquid Sheets, *Phys. Fluids A*, 1990, **2**(5), p 706-719
19. J.C. Lasheras and E.J. Hophinger, Liquid Jet Instability and Atomization in a Coaxial Gas Stream, *Annu. Rev. Fluid Mech.*, 2000, **32**, p 273-308
20. S. Markus, U. Fritsching, and K. Bauckhage, Jet Break up of Liquid Metal in Twin Fluid Atomization, *Mater. Sci. Eng.*, 2002, **A326**, p 122-133
21. N.A. Hussary, J. Schein, and J.V.R. Heberlein, Control of Jet Convergence in Wire Arc Spray Systems, *Tagungsband Conference Proceedings*, E. Lugscheider and R.A. Kammer, Ed., March 17-19, 1999 (Düsseldorf, Germany), DVS Deutscher Verband Für Schweißen, 1999, p 335-339